Flame acceleration and detonation onset in narrow channels: simultaneous schlieren visualization

Yves Ballossier, Florent Virot, Josué Melguizo-Gavilanes

Flame acceleration and detonation onset in narrow channels: simultaneous schlieren visualization

Yves Ballossier*, Florent Virot, Josué Melguizo-Gavilanes*

[a]*Institute Pprime, UPR 3346 CNRS, ISAE-ENSMA, 86961, Futuroscope-Chasseneuil, France*

Abstract

Deflagration-to-detonation-transition (DDT) experiments were performed in a fully optically accessible smooth narrow channel using simultaneous schlieren visualization. Stoichiometric H_2-O_2 mixtures with various N_2 dilution levels were used to assess the effect of expansion ratio on flame acceleration (FA) and detonation onset (DO). Results show that the flame topologies and flame-shock complexes that form prior to transition differ and the corresponding DO modes become less random as dilution is increased. The widely accepted symmetric assumptions during the very early stages of flame propagation are verified whereas complex asymmetric structures are unraveled and described during FA and DO. Using the information collected from the additional visualization direction, the role of asymmetries during FA are highlighted, and maps of the spatial likelihood of detonation onset on the channel's cross section are built. Conclusive experimental evidence of the role played by walls and corners in the formation of ignition centers/hot spots on DDT is provided. The value of simultaneous schlieren visualization in providing unique insight into the reacting front and wave topologies present during the entire DDT evolution is, for the first time, demonstrated.

Keywords: flame acceleration; detonation onset; DDT; simultaneous schlieren visualization; hydrogen safety

*Corresponding author:

Email addresses: yves.ballossier@univ-amu.fr (Yves Ballossier), josue.melguizo-gavilanes@cnrs.pprime.fr (Josué Melguizo-Gavilanes)

Preprint submitted to Combustion and Flame

1. Introduction

Deflagration-to-detonation transition (DDT) continues to be an active topic of research since its discovery. In the late 1800's Mallard & Le Chatelier [1] and Berthelot & Vieille [2] reported an abrupt change in front propagation speed, preceded by a period of intense fluctuations, while studying flame propagation in tubes. It is still important to gain improved understanding of DDT to develop engineering correlations and simulation tools that can be applied to propulsion [3], and the prevention/mitigation of explosions [4].

DDT research progress thereafter, focused primarily on flame acceleration (FA) mechanisms such as the presence of obstacles, shock-/pressure wave-flame interactions due to reflections from walls and associated instabilities (i.e. Richtmyer–Meshkov, Kelvin-Helmholtz), as well as precompression of unburned gases. The Shock Wave Amplication through Coherent Energy Release (SWACER) mechanism [5] was subsequently proposed as a rationalization of detonation onset, following closely the ideas of Zel'dovich [6].

The reviews of Shepherd & Lee [7], and Ciccarelli & Dorofeev [4] summarize all the experimental work done in the 80's, 90's and early 2000's. Notable take-aways are (i) DDT can be divided in two separate problems: (1) FA leading to conditions of detonation onset which is dependent of specific initial and boundary conditions with gas dynamics [8] and flame folding [9] playing a role in the acceleration process; (2) actual detonation onset (DO), which appears to be universal, and involves hot spots, reaction waves, and the amplification of weak shock waves through gradients of induction delay time within the flow; FA and DO are both deemed equally important. (ii) explosions in industrial settings occur through DDT after ignition of a flame by an electric spark or a hot surface. FA is known to be promoted by the increase of flame surface area as a result of its interaction with obstacles and rough walls; self-turbulization of the flame plays an important role in large channels (i.e., those in which the size, δ, of the hydrodynamic boundary layers that develop during FA are much smaller than the characteristic length scale of the channel, L) [10, 11]. In smooth narrow

channels ($\delta \sim L$), FA seems to be promoted by different mechanisms [12] such as intrinsic flame instabilities [13] and viscous heating [14], both increase flame wrinkling and, in turn, its surface area resulting in acceleration of the flame [9]. The review of Oran and Gamezo [15] provides a detailed account of numerical and theoretical work done up until 2007. This work showed the essential role played by shock-flame interactions and hot spots in creating the right conditions for DO to occur: obstacles and hydrodynamic boundary layers through their interactions with shocks and flames result in the development of hot spots [16]. Numerical studies typically require simplifications to make them tractable. One of the most commonly exploited is the use of axial symmetries to reduce resolution requirements [17–19]. However, to the best of our knowledge, this reasonable but rather strong assumption is not supported by experimental evidence. Further experimental, numerical and theoretical contributions were made subsequently attempting to clarify the role of boundary layer, viscous heating, compressibility, unsteadiness and strong flow gradients [19–25]. Whether these effects are essential to DDT or merely aiding mechanisms remains largely unknown.

While all the previous body-of-work has recognized that the deflagration structure just prior to DO, as well as that of the detonation itself is three-dimensional (3-D), surprisingly, no experimental setup has been devised that allows for simultaneous visualization of the phenomenon from two mutually orthogonal directions. Here, we present such a setup and the new experimental data collected during FA and DO for N_2-diluted stoichiometric H_2-O_2. Our article thus provides the first detailed 3-D experimental characterization of FA in a smooth narrow channel from ignition to DO, as well as maps of the spatial likelihood of DO on the channel's cross section as a function of dilution.

2. Experimental setup

The combustion chamber and optical setup allowing simultaneous schlieren visualization were improved based on the learnings from the experimental campaign presented in [26].

Next, we only provide details on the improvements made to the experimental setup.

2.1. Apparatus and procedure

Figure 1 shows an exploded view of the narrow channel together with a cross-sectional view including important manufacturing details (1030-mm $\times$ 10-mm $\times$ 9.4-mm); the cross section's geometric uniformity is ensured by means of retaining walls of 0.6-mm (see detail in Fig. 1 – bottom). The channel walls are 15-mm-thick polycarbonate plates enclosed by aluminum flanges at the top and bottom together with lateral spacers on the sides to avoid bending during detonation onset and subsequent detonation propagation. The structural integrity of the channel is guaranteed with bolts screwed on the aluminum frame in a sandwich-like configuration. Regarding the boundary conditions, the channel is kept closed at the ignition end (inlet) and left open at the opposite end (outlet); see Fig. 1 – top.

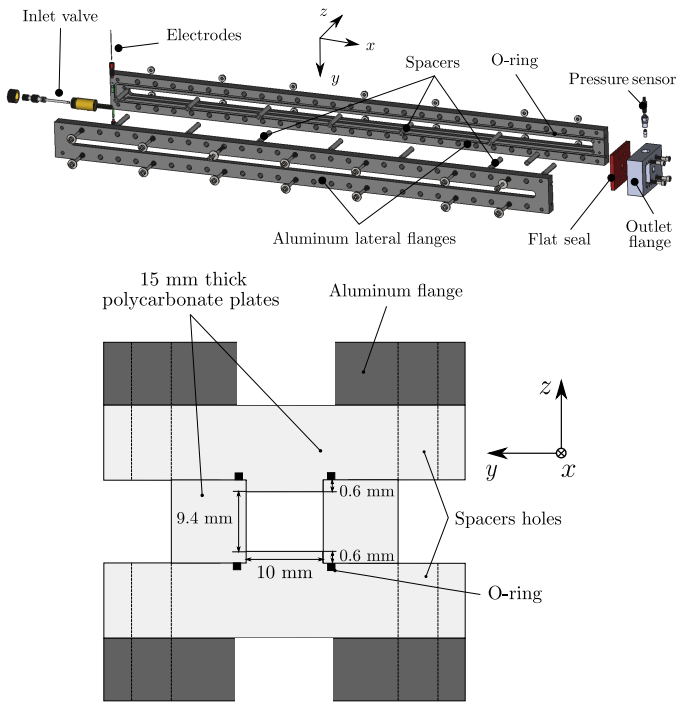

Figure 1: Annotated exploded-view of narrow channel (top) and cross-sectional view (bottom).

The experiments are conducted as follows: (i) the channel is first vacuumed to an absolute

pressure below 10 mbar (controlled by a MKS 220DA pressure sensor); (ii) a plastic cap, held by a servo motor's arm, seals the open end of the channel; (iii) the reactive mixture (prepared and mixed beforehand) is fed into the channel until atmospheric pressure is reached. At this point, the plastic cap is automatically removed by the servo motor; (iv) one second later, the mixture is ignited 3 mm away from the closed end by the electric arc that forms between the two electrodes whose estimated energy, E_{ign}, is approximately 1 mJ. This procedure ensures adequate control of the mixture equivalence ratio ($\Phi = 1 \pm 0.01$) within the channel. In addition, the waiting time between filling and ignition is controlled to 15 s as this was found sufficient to avoid any impact of initial flow unsteadiness on the early stages of flame propagation [27]; (v) to remove any visible condensation from the burned gases the channel is vacuumed for at least three minutes after each test.

2.2. Diagnostics

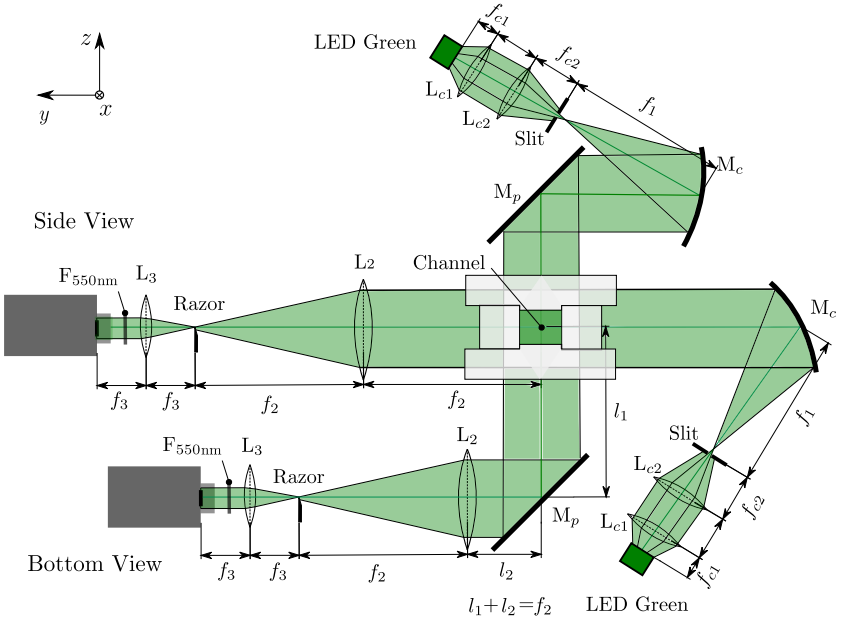

Figure 2: Schematic of the simultaneous schlieren visualization set-up. "Side" and "Bottom" faces refer to the camera position.

High-speed simultaneous schlieren visualization requires an independent set of optics for

each direction viewed. The two cameras used were: (i) a Shimadzu HPVX-2 (bottom view), with acquisition rates ranging from 200,000 (200 ns exposure time) to 10 million fps (50 ns exposure time), and (ii) a Shimadzu HPV-2 (side view) with acquisition rates of 125,000 (1000 ns exposure time) to 1 million fps (250 ns exposure time). Table 1 summarizes the optical configuration shown in Fig. 2. Slit and razor are placed to capture gradients in the direction of flame propagation. The optical layout allows for resolutions of 111 μm/pixel and 106 μm/pixel to visualize 34.6 mm (side) and 42.5 mm-long (bottom) sections, respectively. The resolutions are 312 pixels (horizontal) and 90 pixels (vertical) for both views to match the smallest field of visualization. Cameras are from different generations resulting in discrepancies in sensitivity and level of details provided on different views.

Table 1: Optical focal lengths in mm for visualization directions shown in Fig. 2.

View	Side	Bottom
Condenser (f_{c1} / f_{c2})	75 / 150	75 / 150
Collimator (f_1)	500	500
Focal length (f_2)	500	500
Collector (f_3)	150	300

A complete characterization of the flame acceleration dynamics is carried out by keeping the optics fixed and translating the channel. At least two shots per section and per dilution were performed to assess repeatability, and approximately 20 shots per dilution in sections where detonation onset occurred. The experimental campaign comprised a total of 310 shots, all mixtures and sections included. Additionally, due to the intense chemiluminescence during detonation onset, hard-coated short-pass filters (Thor Labs Ref. FESH0550) were used between the set of collector lenses and the high-speed cameras; with a cut-off wavelength below 400 nm and above 550 nm, the filters do not affect the acquired images from the LED's emission but avoid saturation of the cameras' sensors. Green 20-W monochromatic LEDs are used as light sources. Finally, both high speed cameras are triggered from the signal emitted by a photo-diode (BPW34) placed at the start of the section tested.

3. Results and discussion

The experimental campaign included the characterization of FA from ignition to DO for five N_2 dilutions in $2H_2$+O_2+ηN_2 mixtures (η = 0, 1, 2, 2.5, 3.76). Table 2 lists properties such as the laminar burning velocity S_L, expansion ratio $\sigma = \rho_0/\rho_b$, Zel'dovich number $\beta = E_a/R_u T_b(T_b - T_0)/T_b$, thermal flame thickness ($\delta_t = (T_b - T_0)/(\nabla T)_{\max}$), detonation induction length l_{ind}, and Chapman-Jouguet detonation velocity D_{CJ}, for all the mixtures tested. The reported values were computed using Cantera [28] and the Shock and Detonation Toolbox [29] with the detailed mechanism of Mével [30, 31]. The methodology used to determine the effective activation energy E_a/RT_b can be found in [32]. In the expressions above ρ, T and R_u are the density, temperature, and universal gas constant, respectively; subscripts 0 and b refer to fresh and burnt mixture. Also included in Table 2 is whether or not DDT occurred in our 1-m long channel. Only $\eta = 0$ and 2 are discussed next as these are representative of the transition to detonation dynamics observed in the available channel length.

Table 2: Combustion properties of the N_2-diluted stoichiometric H_2-O_2 mixtures studied. Initial conditions: $p_0 = 100$ kPa, $T_0 = 300$ K and $2H_2$+O_2+ηN_2.

η	% $N_{2,\text{vol}}$	S_L (m/s)	σ	β	δ_t (mm)	l_{ind} (μm)	u_{CJ} (m/s)	DDT
0	0	10.46	8.25	2.82	0.22	34	2834	Yes
1	25	6.46	7.90	2.86	0.27	51	2394	Yes
2	40	4.36	7.55	2.94	0.32	75	2184	Yes
2.5	45.5	3.64	7.35	3.05	0.34	90	2110	Yes
3.76	55.6	2.39	6.79	3.31	0.37	144	1968	No

3.1. $x - t$ diagrams

Flame tip positions are detected from schlieren visualization taken at different sections of the channel and are the result of at least 44 tests per dilution. Figure 3 shows $x - t$ diagrams for η = 0, 1 and 2. These diagrams allow to determine the average DDT run-up distance, $\bar{x}_{\text{DDT}}$, and time, $\bar{t}_{\text{DDT}}$, i.e., distance/time from ignition to detonation onset

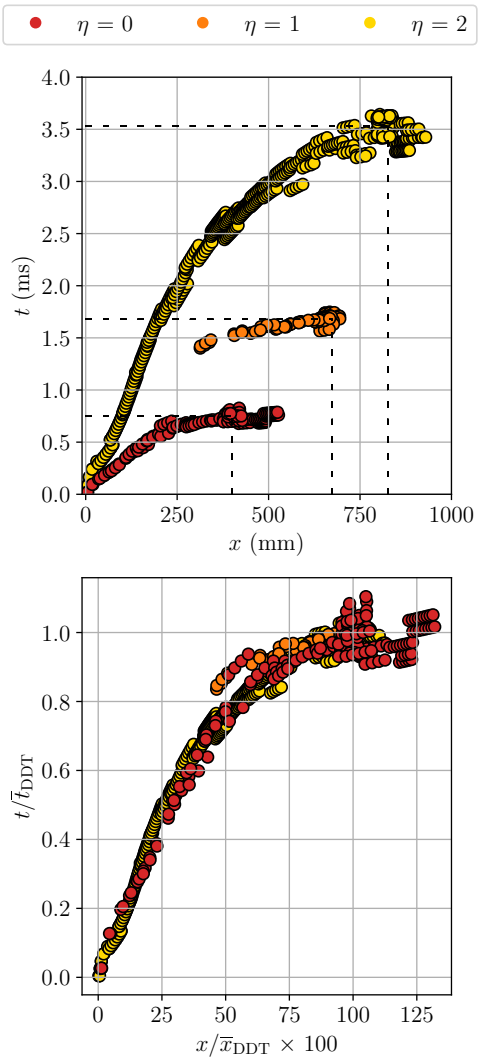

Figure 3: $x - t$ diagrams for $2H_2 + O_2 + \eta N_2$ at $p_0 = 100$ kPa, $T_0 = 300$ K. DDT run-up distances and times are: $\bar{x}_{\mathrm{DDT}} = 399.2$ mm, $\bar{t}_{\mathrm{DDT}} = 748\,\mu$s for $\eta = 0$; $\bar{x}_{\mathrm{DDT}} = 674$ mm, $\bar{t}_{\mathrm{DDT}} = 1.680$ ms for $\eta = 1$; $\bar{x}_{\mathrm{DDT}} = 826$ mm $\bar{t}_{\mathrm{DDT}} = 3.532$ ms, for $\eta = 2$.

(shown as dotted lines) whose values are included in the figure caption. The bottom figure is normalized by $\bar{x}_{\mathrm{DDT}}$, and $\bar{t}_{\mathrm{DDT}}$. Note that upon normalization the lines collapse suggesting that comparisons among dilutions can be made at the same stage of the DDT evolution. The early stages of the FA process was not measured for $\eta = 1$ since we restricted our attention to the moments just before detonation onset for this dilution level.

3.2. Flow topologies during FA

In Figs. 4 to 13 each frame is composed of two sub-frames including the "Side" (xz-plane) and "Bottom" (xy-plane) views. The horizontal axis displays the section along which the simultaneous visualization is performed relative to detonation onset, i.e., $x/\overline{x}_{\mathrm{DDT}} \times 100$. The time stamps above each frame indicate the time elapsed from the first frame shown in the sequence. To obtain similar gray-scales in the figures, the raw images recorded by both cameras were post-processed by matching their histograms and resolution; performing a frame-by-frame subtraction of the average field obtained over the sequence collected; followed by a color inversion. The aforementioned steps were automated via a Python script, and the leftover noise ahead of the flames/precursor shocks was manually removed. The final images were carefully checked and compared with the original videos afterwards to ensure that no artifacts were mistakenly produced as a result of our post-processing scheme. The entire FA process, from ignition to DO, is shown in detail for $\eta = 0$ and 2.

3.2.1. Early stages - $9 \lesssim x/\overline{x}_{\mathrm{DDT}} \times 100 \lesssim 30$

Once ignited at the center of the channel, near the close end, spherical flame kernels propagate due to the combined effect of fresh reactants consumption, burnt products expansion and geometrical confinement. The presence of a closed end promotes a pressure build up that pushes the flames towards the open end, increasing their surface area, associated consumption rates and therefore, results in their abrupt acceleration. Initially, laminar finger-flame topologies [33–38] are observed for all dilutions, followed by flame flattening due to interaction between flame skirt and walls, slowing down the flame, and eventually inverting it.

Two-direction visualization verifies the symmetry of the flames during the first acceleration/deceleration phase of propagation. However, N_2 dilution is observed to significantly affect the flame topology. For $\eta = 0$, the combined effect of a higher laminar flame speed

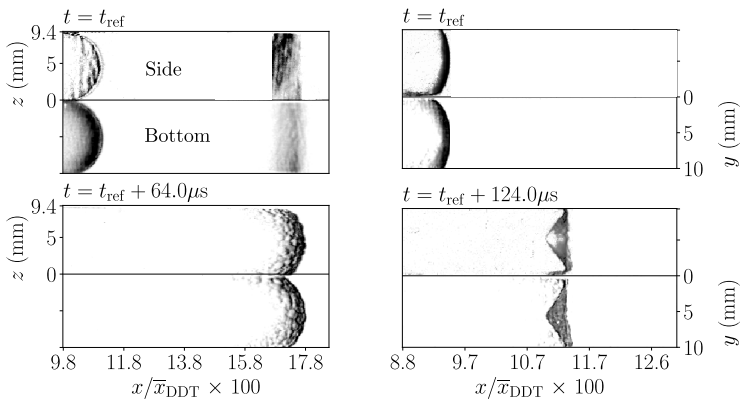

(a) $\eta = 0$ (b) $\eta = 2$

Figure 4: Simultaneous schlieren visualization of initial stage of flame acceleration for $2H_2+O_2+\eta N_2$ at $x/\overline{x}_{\mathrm{DDT}} \times 100 \sim 10$. Initial conditions $p_0 = 100$ kPa, $T_0 = 300$ K.

and expansion ratio lead to the formation of a precursor shock, whose early stages are visible in Fig. 4 (a). Small scale Darrieus-Landau (DL) instabilities develop on the flame surface, resulting in larger overall burning rates than those recorded for $\eta = 2$. For the latter dilution, the flame goes though a smooth inversion process, shown in Fig. 4 (b), which has been argued to be mostly driven by hydrodynamic effects [39]. Higher dilutions, $\eta = 2.5$ and $\eta = 3.76$ (not shown), exhibit similar topologies and behaviors as $\eta = 2$, except that front flattening and inversion occur later in time.

In the $\eta = 0$ case, deceleration is delayed by the flow induced by the precursor shock and surface area increase due to instrinsic instabilities. The cut-off wavenumber for the development of DL instabilities is larger for undiluted mixtures [40], meaning that small wavelength perturbations that are unstable for $\eta = 0$ may be stable for $\eta = 2$; local pressure fluctuations could also trigger DL earlier for higher expansion ratios ($\eta = 0$) by local reduction of the laminar flame thickness, δ_t.

The scaling proposed by Valiev et al. [35] collapses the experimental data for all dilutions during the symmetric acceleration/deceleration phase (see $X_{\mathrm{tip}}/R \leq 5$ in Fig. 5; R being half the hydraulic diameter of the channel) but it predicts an earlier deceleration as dilution

decreases. For $\eta = 3.76$ (shown for completeness) the temporal evolution is well captured up to $X_{\text{tip}}/R \sim 25$. Note that in [35] the authors assumed rotational symmetry in their derivation, which is verified by our observations at early stages, but their theory does not account for flame surface instabilities. As soon as the flame develops instabilities (see Fig. 4 (a)) and asymmetries (see Fig. 6), their theory expectedly fails to capture the re-acceleration induced by the increase in flame surface area. Thereafter, flame positions diverge as shown in Fig.5, and scaling with $\overline{x}_{\text{DDT}}$ seems to be more relevant as the flame continues to accelerate towards DO as shown in Fig. 3. While the development of instabilities is the main mechanism that increases the flame surface for $\eta = 0$, smooth flame inversion is a characteristic feature of cases that contain N_2 in channels of the size considered here. Asymmetries however, develop differently for increasing dilution, leading to incipient inversion of an already perturbed flame for $\eta = 0$, and to the appearance of flame surface instabilities of an already inverted flame for $\eta = 2$. For both mixtures the end of the initial deceleration phase is marked by the breakdown of symmetry (see Fig. 6); as the flames move forward towards DO, their shape remains highly asymmetric.

For $\eta = 0$, the flame shape switches from an essentially flat corrugated front to an asymmetric front with preferential burning within a corner (i.e., $z = 0$ mm and $y = 10$ mm for the test shown in Fig. 6 (a)); the front starts a flame inversion process different than the smooth symmetric evolution described earlier. For $\eta = 2$, the smooth concave tulip flame starts to develop small scales instabilities resulting in the stretched, inverted asymmetric flame displayed in Fig. 6 (b). The side view shows that a trail of unburned mixture is located at a wall (top one, $z = 9.4$ mm, on Fig. 6 (b)); the bottom view shows remnants of the tulip flame as two persisting lobes at $y = 0$ and 10 mm. The information collected from the additional direction allows to identify that the lobes propagate within corners (see Fig. 6 (b)) leaving the vicinity of the channel's centerline with unreacted mixture. Note that having only one direction available for visualization would have led to an incomplete picture

of the flame shape as it would not had been possible to identify the unburnt mixture in the channel's centerline. This illustrates clearly the added value of the technique proposed to reveal the actual flame topology during FA.

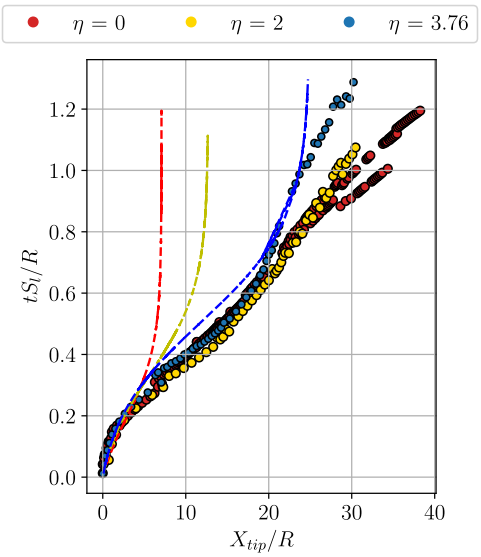

Figure 5: Normalized flame tip position X_{tip}/R vs. front velocity tS_L/R during early stages of propagation. Dashed lines: theoretical prediction from [35]. Symbols: experimental data. Initial conditions $p_0 = 100$ kPa, $T_0 = 300$ K.

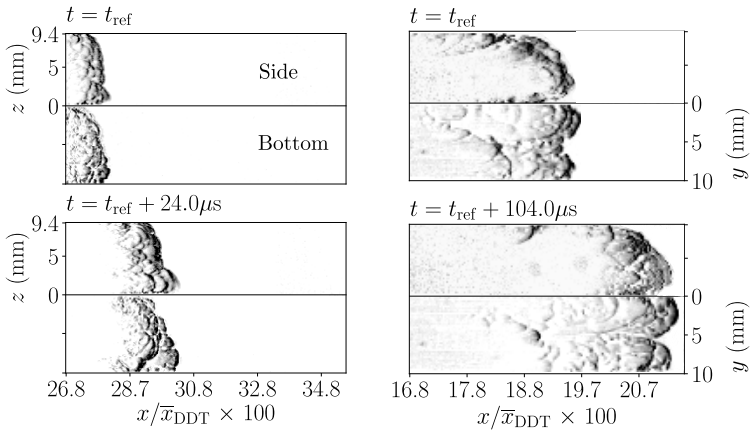

(a) $\eta = 0$ (b) $\eta = 2$

Figure 6: Simultaneous schlieren visualization of early stages of flame acceleration for $2H_2$+O_2+ηN_2 at $x/\overline{x}_{\text{DDT}} \times 100 \sim 20$. Initial conditions $p_0 = 100$ kPa, $T_0 = 300$ K.

3.2.2. Intermediate stages - $35 \lesssim x/\overline{x}_{\mathrm{DDT}} \times 100 \lesssim 70$

Following the end of the symmetric stage, all dilutions experience a quasi-steady acceleration phase (between Fig. 6 and Fig. 7) followed by a sharp increase in acceleration (Fig. 8); the corresponding flame shapes are shown in the above mentioned figures.

Comparing both dilutions at $x/\overline{x}_{\mathrm{DDT}} \times 100 \sim 40$ (see Fig. 7), flames for $\eta = 0$ burn asymmetrically with a trail of fresh gas trapped between the flame surface and a wall (the top wall for the case shown in Fig. 7 (a)) whereas the tips of the flames for $\eta = 2$ (Fig. 7 (b)) form a convex corrugated shape whose overall topology is similar to the one described in the previous subsection (Fig. 6 (b)), with unburned mixture also trapped closed to a wall ($y = 0$ mm), except that the lobes were consumed/absorbed by the growing reaction front and start a re-inversion of the flame. Flame shapes are for the most part similar for $\eta = 0$ and 2 at this stage, a notable difference is that the tip of the flame remains sharper on the side view for $\eta = 0$ whereas an equivalent structure is present in the bottom view for $\eta = 2$. Both flames exhibit a trail of unburned mixture that grows two-fold as the flame continues to accelerate in the channel. Further in the propagation ($60 \lesssim x/\overline{x}_{\mathrm{DDT}} \times 100 \lesssim 70$), the flame asymmetries for $\eta = 0$ remain very significant with preferential combustion along the lower wall ($z = 0$ mm); in Fig. 8 (a), a trail of fresh gas is also present along the center of the upper wall ($z = 9.4$ mm, $y = 5$ mm). On the other hand, for $\eta = 2$, the re-inversion process is over and the flame burns preferentially along the channel's centerline, surrounded by unburned mixture. Other than the small bifurcation at the tip of the flame (not visible from the side view) diluted flames exhibit an overall finger-like corrugated symmetric shape. While FA is mostly promoted by surface area increase for all dilution levels, it is due to asymmetric growth of the trail of unburnt reactants for $\eta = 0$, and to re-inversion and stretching of the symmetric convex flame for $\eta = 2$. The same observations hold for $\eta = 1$ and 2.5, respectively (not shown). However, flame stretching alone may not be enough to explain the sharp acceleration process that starts in Fig. 8 for $\eta = 0$ resulting in an order of

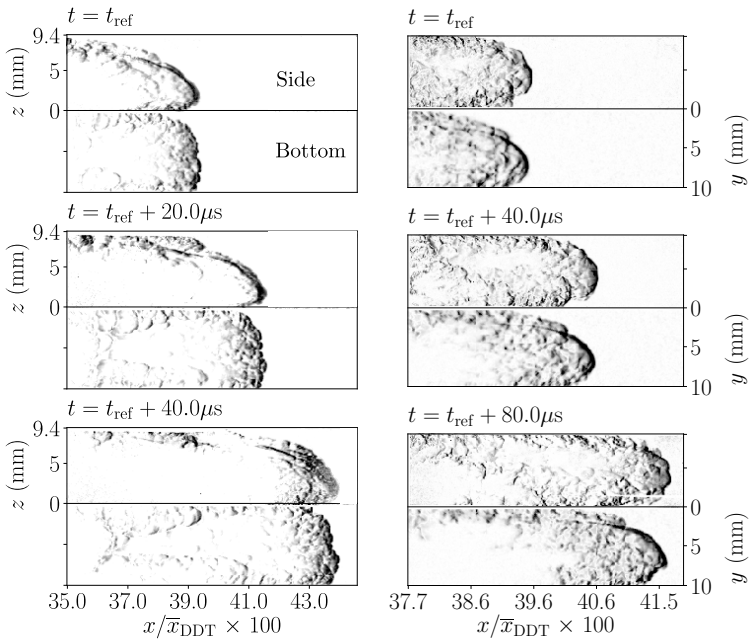

(a) $\eta = 0$ (b) $\eta = 2$

Figure 7: Simultaneous schlieren visualization of intermediate stages of flame acceleration for $2H_2$+O_2+ηN_2 at $x/\overline{x}_{\mathrm{DDT}} \times 100 \sim 40$. Initial conditions $p_0 = 100$ kPa, $T_0 = 300$ K.

magnitude increase in acceleration when compared with the preceding section of the channel (1.5×10^6 m/s^2 to 1.4×10^7 m/s^2); similar observations were reported in [41]. Furthermore, recent experimental and numerical analyses [42] suggest that flame folding alone may not be sufficient either to generate the sharp flame acceleration observed prior to DO. Instead, the authors allude to the combined role of friction and flame wrinkling as the likely mechanisms that trigger the exponential acceleration typical of the late stages of DDT; similar to the individual observations made by Deshaies & Joulin [9], and Brailovsky & Sivashinsky [43] in their work.

3.2.3. Late stages - $78 \lesssim x/\overline{x}_{\mathrm{DDT}} \times 100 \lesssim 96$

To highlight important flow features, such as the formation of pressure waves ahead of the flame, the background subtraction is no longer performed during the image postpro-

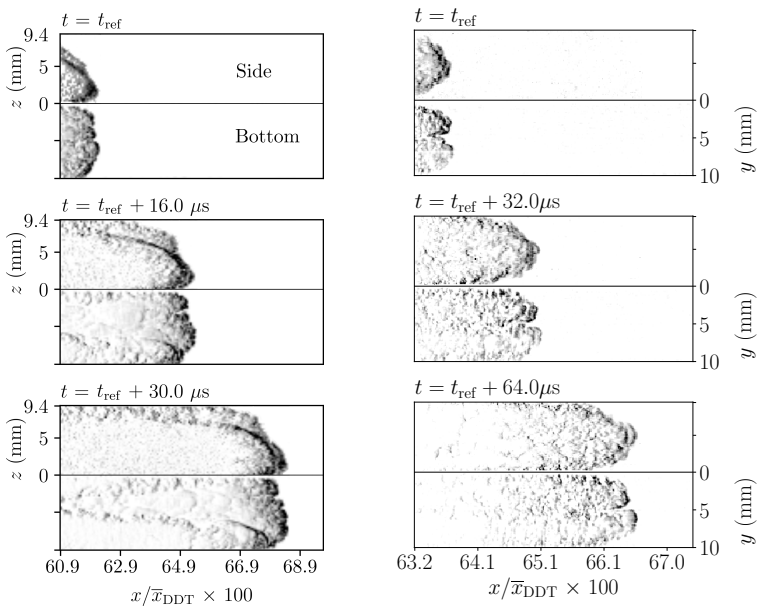

(a) $\eta = 0$ (b) $\eta = 2$

Figure 8: Simultaneous schlieren visualization of intermediate stages of flame acceleration for $2H_2$+O_2+ηN_2 at $x/\overline{x}_{\mathrm{DDT}} \times 100 \sim 60$. Initial conditions $p_0 = 100$ kPa, $T_0 = 300$ K.

cessing. Fig. 9 shows the acceleration of the flame that generates pressure disturbances that subsequently coalesce into shocks. These disturbances are clearly visible for $\eta = 0$, and less visible for $\eta = 2$ due to the higher expansion ratio of the former mixture, as well as the reduced optical quality of the walls after being subjected to successive detonations; the videos provided as supplementary material allow to visualize the aforementioned perturbations more clearly. For $\eta = 2$, the flame stays overall symmetric as described in the section corresponding to $x/\overline{x}_{\mathrm{DDT}} \times 100 \sim 60$ (Fig. 8 (b)). The flame for $\eta = 0$ continues its asymmetric propagation burning faster in one corner, that changes from test to test, and that always results in a localized trail of unburnt gas forming a conical flame.

Figure 10 compares the flame topologies for $\eta = 0$ and 2. The later stages of flame acceleration are characterized by the formation of a shock induced preheated zone [44] visible between the precursor shock and the flame brush denoted by Z_{PH}. For $\eta = 0$ (Fig. 10 (a)) the flame exhibits a conical shape up until detonation onset with a rather

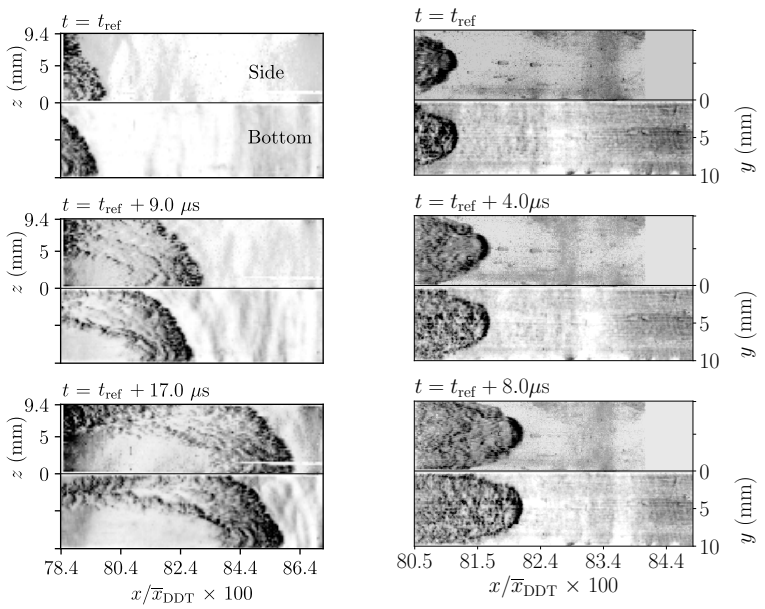

(a) $\eta = 0$ (b) $\eta = 2$

Figure 9: Simultaneous schlieren visualization of the late stages of flame acceleration shock wave formation for $2H_2$+O_2+ηN_2 at $x/\overline{x}_{\mathrm{DDT}} \times 100 \sim 80$. Initial conditions $p_0 = 100$ kPa, $T_0 = 300$ K.

large preheated zone length of $Z_{\mathrm{PH}} \sim 0.03 - 0.035\overline{x}_{\mathrm{DDT}}$ ($12 - 14$ mm measured from the tip of the flame). While the flame topology is similar to the waffle cone structure observed in tubes with larger cross-sections [45], our simultaneous two-directional schlieren visualization allows us to reveal the complex flow structure present during its propagation. Successive pressure waves generated by the accelerating flame trail the precursor shock, and propagate faster than the flame itself. These waves catch up with the precursor shock reinforcing pressure build-up in the preheated zone and thus facilitating flame propagation in a fresh but shocked mixture at higher pressure and temperature. This feedback between flame acceleration and shock induced pressure build-up reduces Z_{PH}. The features just described characterizing the late stages of FA were shown to be qualitatively reproduced by a simple one-dimensional model including friction losses in [25] and suggest a plausible mechanism responsible for front acceleration. For $\eta = 2$ (Fig. 10 (b)) the preheated zone is significantly smaller, $Z_{\mathrm{ph}} \sim 0.005\bar{x}_{\mathrm{DDT}}$ (~ 4.13 mm). Again, the reduced image quality is due to the large

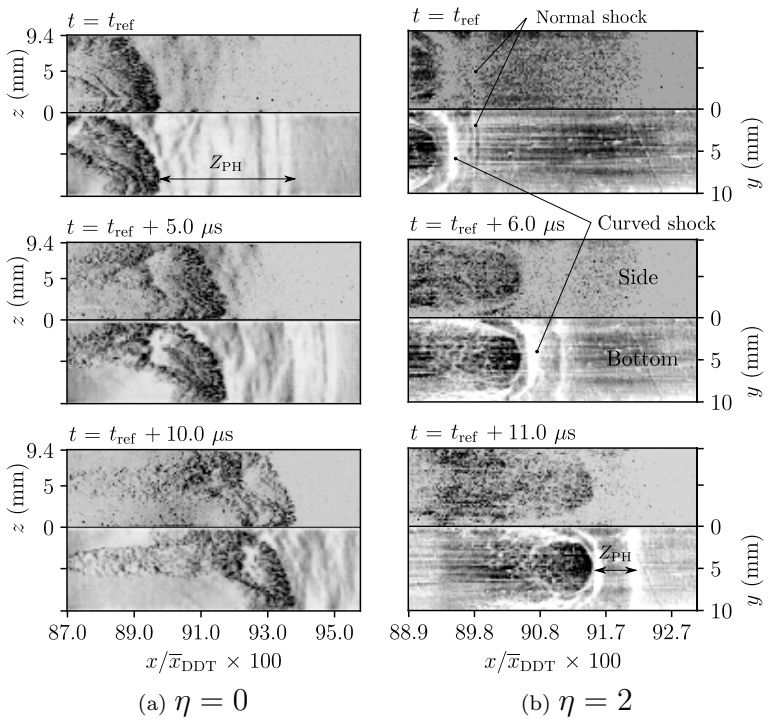

Figure 10: Simultaneous schlieren visualization of late stages of flame acceleration for $2H_2$+O_2+ηN_2 at $x/\overline{x}_{\mathrm{DDT}} \times 100 \sim 90$. Initial conditions $p_0 = 100$ kPa, $T_0 = 300$ K.

number of tests performed and the fact that this section of the channel ($\sim$ 750 mm from ignition) has been exposed to fully established detonations most of the time, hence very high pressures and temperatures, that diminish the optical quality of the polycarbonate walls. This results in strong diffusion of the collimated light beam, which in turn worsens the schlieren visualization.

For this dilution the flame is not followed by entrained unburned mixture in the centerline of the channel. Instead, a symmetric ogive-like corrugated flame generates curved pressures waves, forming a pre-heated zone in close proximity to itself but behind the leading precursor shock. Secondary shocks are no longer planar but observed to be curved and form closer to the flame. This is visible in all frames of Fig. 10 (b). The tip of the flame is aligned with the longitudinal axis of the channel. At this stage, detonation onset is imminent.

The role of turbulence during all the stages of FA is difficult to assess quantitatively.

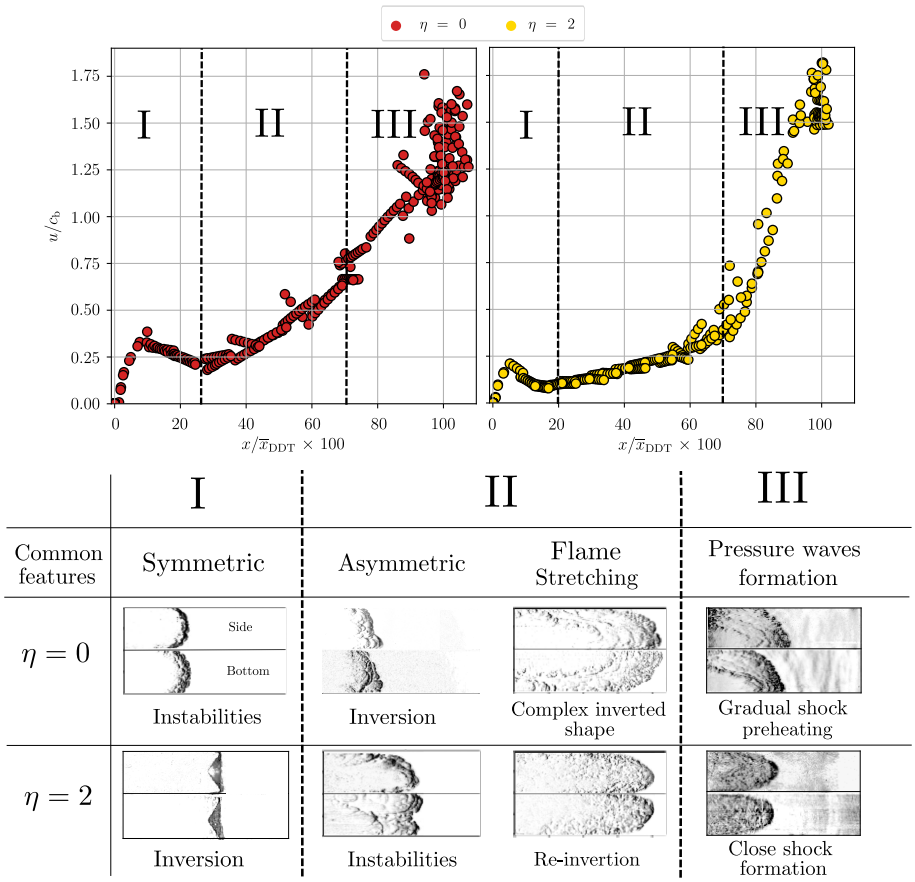

Figure 11: Top: Flame tip velocity, u_f normalized by the sound speed in burned products, c_b as a function of flame tip position relative to distance to DDT. $\eta = 0$: $c_b = 1449$ m/s; $\eta = 2$: $c_b = 1126$ m/s. Initial conditions $p_0 = 100$ kPa, $T_0 = 300$ K. Bottom: summary of the FA stages and flame topologies prior to DO.

However, it can be estimated via planar shock relations (one shock for $\eta = 2$, and successive shocks for $\eta = 0$) to determine a flow velocity ahead of the accelerating flame. The flow Reynolds number, Re, based on the height of the channel lies between 5×10^5 and 7×10^5. These Re numbers are characteristic of turbulent flow, but the flame-shock distance may not be enough to result in laminar-to-turbulent transition in the shock induced boundary layer. All in all, while it is plausible that turbulence plays an aiding role in the observed FA for all dilutions considered, intrinsic flame instabilities seem to be a more (or an equally) important FA mechanism in the narrow channel at hand.

Figure 11 (top) shows flame tip velocities normalized by the sound speed in burned

products (u_f/c_b) for $\eta = 0$ (left) and $\eta = 2$ (right), along with a summary of the FA stages and flame topologies prior to DO (Fig. 11 bottom). The maximum values reported do not therefore account for the over-driven stage shortly after DO that reach values as high as $3c_b$ before relaxing to $u_{\mathrm{CJ}} \sim 2c_b$, or even lower values due to the known deficits present in narrow channels [26]. For $\eta = 0$, u/c_b increases almost linearly in the interval $30 \lesssim x/\overline{x}_{\mathrm{DDT}} \times 100 \lesssim 90$. For $\eta = 2$ a different trend is observed, a linear u/c_b evolution over $20 \lesssim x/\overline{x}_{\mathrm{DDT}} \times 100 \lesssim 70$ followed by a sharp increase linked to the development of pressures waves as illustrated by the flame topologies highlighted previously. After the early stage (I), non diluted flames show asymmetric shapes until DO; a train of pressures waves between the flame and the precursor shock generates a large preheated zone, Z_{PH}. The unchanged flame topology and gradual shock induced preheating result in a progressive u/c_b increase for increasing $x/\overline{x}_{\mathrm{DDT}}$. For $\eta = 2$ the asymmetric phase is followed by a re-inversion to a corrugated symmetric shape. Late development of pressure waves and shock formation occurring around $x/\overline{x}_{\mathrm{DDT}} \times 100 \sim 70$ results in the drastic change of slope visible in Fig. 11 top for $\eta = 2$; the same holds for $\eta = 2.5$. Likewise, $\eta = 1$ exhibits a similar trend as that of $\eta = 0$. Diluted flames propagate at higher u/c_b just before DO; shock induced preheating is not as strong and may explain this observation. Note that in the $\eta = 2$ case, due to longer propagation times for a fixed channel length (1 m), flame interactions with expansion waves reflecting from the open end are possible around $x/\overline{x}_{\mathrm{DDT}} \times \sim 90$; for lower dilutions, the aforementioned interactions occur after DO, or, in the $\eta = 0$ case do not occur at all, instead, the detonation catches up any pressure perturbations that develop early during the FA process.

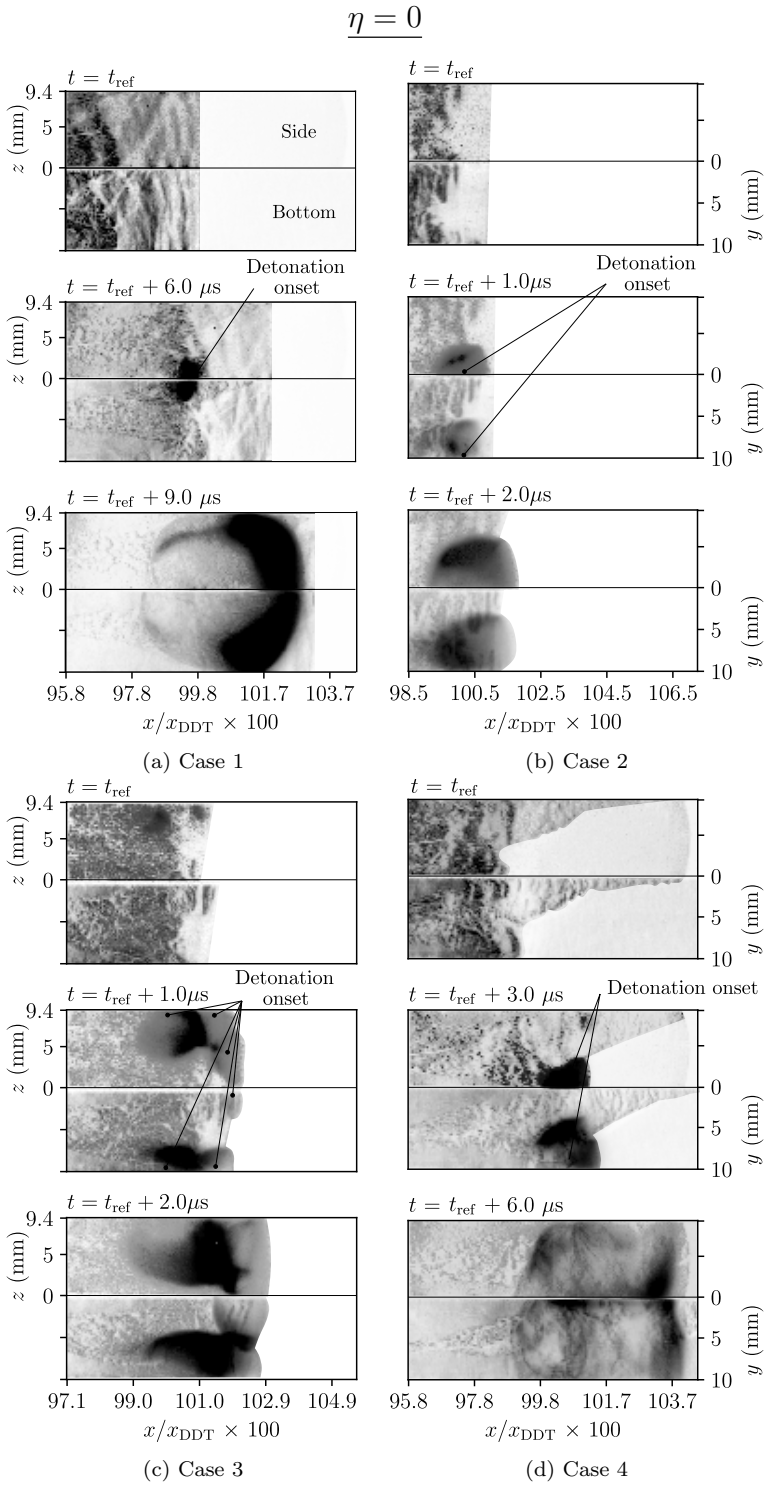

Figure 12: Modes of detonation onset (DO) captured with simultaneous schlieren visualization for $2H_2+O_2+\eta N_2$ with $\eta = 0$. Run-up distances are $x_{\mathrm{DDT}} = 396$ mm (Case 1), 403 mm (Case 2), 409 mm (Case 3), 401 mm (Case 4).

3.3. Detonation onset

3.3.1. DO scenarios for varying dilutions

As the flame gains ground within the preheated zone (see Fig. 12 (a), case 1 $\eta = 0$; $t = t_{\mathrm{ref}}$), favorable thermodynamic conditions are achieved for the mixture to ignite in the subsequent frame at $t = t_{\mathrm{ref}} + 6$ μs. The spherical blast wave that results from the explosion process overtakes the preheated zone, interacts with the flame and the unreacted mixture entrained between its surface and the walls to finally couple with the leading precursor shock to form a detonation wave. Surprisingly, the side and bottom views do not show obvious differences but asymmetries in flame topologies continue to be present. An interesting example of the utility of two-direction visualization is the ability to pinpoint the exact location of the detonation onset: at a corner. While it appears to have taken place behind the flame tip in the bottom view, ignition of the mixture actually occurs at the edge of the flame (see Fig. 12 (a) at $t = t_{\mathrm{ref}} + 6$ μs).

Additional less frequent detonation onset scenarios were also captured with this mixture. Similar to case 1 the flame stays conical but advances further into the preheated zone prior to DO. As the flame and precursor shock start to merge, one (Fig. 12 (b)) or several (Fig. 12 (c)) ignition centers form simultaneously close to walls. These cases illustrate detonation initiation due to flame-shock and flame-boundary layer interactions; $\eta = 1$ resulted in similar flame-shock complexes prior to transition (not shown). Recent numerical research on DDT [46, 47] confirm the aforementioned mechanisms emphasizing the importance of local pressure increments close to the flame front and/or viscous heating as crucial components of the DDT process. Note that the formation of a preheated zone is not a sufficient condition for DO as shock induced preheating alone does not reduce significantly the induction delay time [48]. However, recent theoretical work [49], and an experimentally informed simulation [50] revealed the crucial role of compressibility and the importance of the late stages of

FA in the potential development of very strong shocks in close proximity to the flame front than subsequently leads to DO.

Figure 12 (d) shows a completely different detonation onset. Confining an undiluted stoichiometric H_2-O_2 mixture is technically challenging. Due to its high mass diffusivity, fresh mixture can fill small regions/gaps outside the channel and burn without quenching as long as the size of the gap is of the order of or larger than the laminar thermal flame thickness of the mixture, δ_t. The successive pressure build up from the FA process, may cause slight bending of the polycarbonate allowing for fresh mixture to diffuse away. A sign of this phenomenon is visible as a reaction front that runs obliquely along a corner up to the leading precursor shock. We emphasize that this outcome was not observed with diluted mixtures likely due to actual flame quenching as a result of having larger thermal flame thicknesses for increasing N_2 dilution, or to the less significant pressure build-up during flame acceleration as a result of their lower expansion ratios. Note that this detonation onset scenario may be more representative of the expected evolution during an accidental ignition event.

Figure 13 shows a typical transition event for $\eta = 2$. The most notable differences with the non-diluted cases are: (i) the initially curved shock flattens and the heating induced due to its interaction with the corners ignites symmetric oblique flames within the boundary layer that meet with the curved, corrugated reaction front that propagates along the channel's centerline (see $t = t_{\mathrm{ref}}$); (ii) this shock-flame complex gradually starts to catch up with the precursor shock, however, DO occurs at the wall, close to the shock, before merging (see $t = t_{\mathrm{ref}} + 3\,\mu$s). While flame-/shock- boundary layer interactions were found to be the main mechanisms leading to DO across the dilutions studied, the nature of this interaction is of a different type for increasing dilution. The oblique flames propagate faster within corners through the preheated zone, unable to burn beyond this region, the flame is confined to propagate through the center of the channel further compressing the preheated zone prior

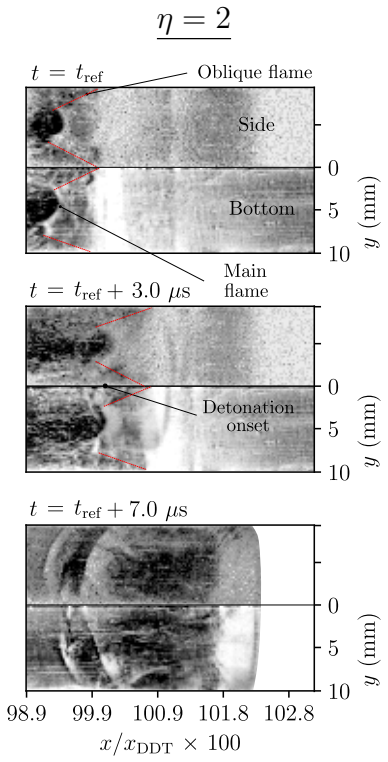

Figure 13: Detonation onset captured with simultaneous schlieren visualization for $2H_2+O_2+\eta N_2$ with $\eta = 2$. Run-up distance is $x_{\mathrm{DDT}} = 823$ mm.

to DDT. This flame topology was observed numerically in [19] using a smaller channel (2 mm) with adiabatic walls and stoichiometric H_2-O_2 but to our knowledge never reported experimentally. The overall DO structures were more repeatable for $\eta = 2$ than for $\eta = 0$; $\eta = 2.5$ resulted in similar flame topologies prior to leaving the optically accessible section.

Our results suggests that DO occurs following flame interactions with the shocks trapped between the flame, the channel's walls and the leading precursor shock. For undiluted stoichiometric H_2-O_2 the DO dynamics displayed some variation; in total four distinct cases were observed. As dilution was increased however, detonation onset appeared to be less random and more repeatable scenarios took place. Sample videos of the dynamics just mentioned are included as supplementary material. We note that the DDT point is observed to be preferentially located within corners, but not always at the same corner. Additional details

on the spatial distribution of detonation onset are discussed in the following subsection.

3.4. Spatial distributions on channel's cross section

The additional information collected from the second visualization direction allow us to draw maps of detonation onset likelihood on the channel cross section. Figure 14 shows these maps for $\eta = 0$, 1 and 2 which include sample sizes of 22, 20 and 22 shots, respectively. The likelihood of DO was quantified by partitioning the channel's cross-section in 25 regions (i.e., a 5×5 grid), counting the number of DO events that occurred in each region, dividing it by the total number of tests carried out per dilution, and multiplying it by a 100 to express it as a percentage. An important feature stands out, DO was never observed to occur in the core of the channel regardless of dilution level (total sample size: 64 tests) but always took place on walls with corners being the most likely location.

The maps for $\eta = 0$ and 1 present a similar distribution although the face $z = 0$ mm contains most of the initiations for the latter. For $\eta = 2$ DO occurs mostly on the wall located at $z = 9.4$ mm with a large proportion ($\sim 50\%$) within the corner ($y = 0$ mm, $z = 9.4$ mm). The resemblance of the DO maps for $\eta = 0$ and 1, and the stark difference in the spatial distribution for $\eta = 2$ may be explained by the variability in flow structures observed prior to DO for the former, and the more repeatable onset resulting in a more limited distribution for the latter.

The spatial distribution of DO seems to be a function of dilution and may be the result of the different flow structures that develop before transition, we note however that a larger data set may plausibly change the distributions obtained; we are currently performing additional tests to verify this statement. These observations provide further evidence of the role played by walls on DO, most probably through the formation of favorable thermal gradients [51, 52] due to friction induced heating within the hydrodynamic boundary layer [23, 25, 53]. The formation of ignition centers within corners was conclusively confirmed by our results in line

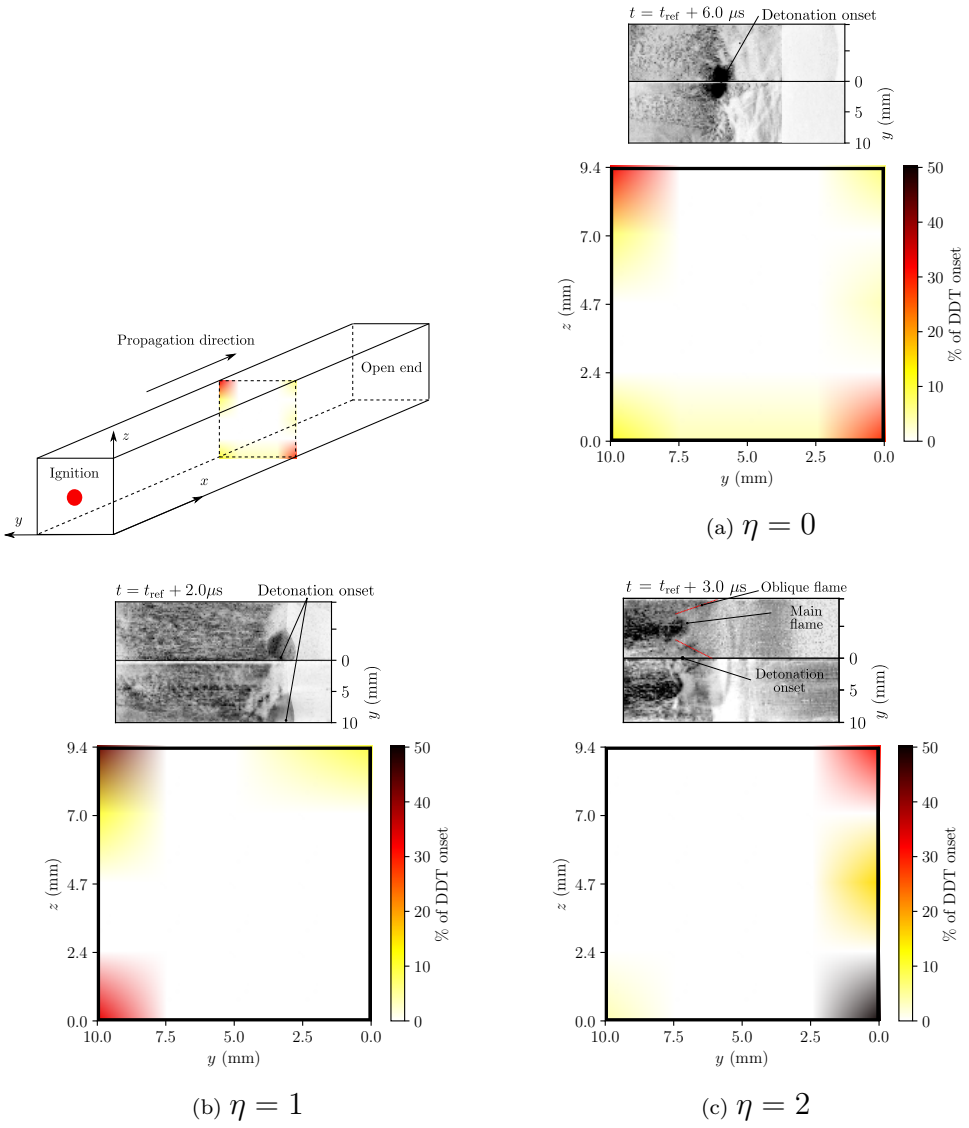

(a) $\eta = 0$

(b) $\eta = 1$

(c) $\eta = 2$

Figure 14: Spatial likelihood of detonation onset on the channel cross section and representative flow structures prior to DDT for $2H_2+O_2+\eta N_2$ at $p_0 = 100$ kPa, $T_0 = 300$ K. Sample size: 22 tests for $\eta = 0$, 20 tests for $\eta = 1$, and 22 tests for $\eta = 2$.

with recent experiments [26]; the spatial distributions measured do not therefore seem to be facility dependent.

4. Conclusion

An experimental study on flame acceleration and detonation onset in a fully optically accessible smooth narrow channel was performed using simultaneous schlieren visualization.

$2H_2+O_2+\eta N_2$ mixtures were employed to assess the effect of expansion ratio on flame acceleration and detonation onset. The flame topology and flame-shock complexes showed significant differences during flame propagation/acceleration and just before transition to detonation yielding more random onset scenarios for $\eta = 0$ and 1 than for $\eta = 2$. All dilutions studied experience an initial symmetric stage driven by hydrodynamics triggering flame surface instabilities for low N_2 dilution, and flame inversion for high N_2 dilution. Development of asymmetries mark the end of the hydrodynamic phase and the beginning of a quasi-steady acceleration phase where all dilutions display a similar topology. Re-acceleration of the flame is then promoted by flame stretching exhibiting asymmetric shapes for $\eta = 0$, and re-inversion to a corrugated symmetric flames for $\eta = 2$. This re-acceleration results in pressure perturbations that are strong enough to form shocks and a shock induced preheated zone, rather large for $\eta = 0$ due to earlier shock formation, and shorter for $\eta = 2$ due to late shock formation attributed to its lower expansion ratio. DO occurred near the flame front through one or several ignition centers. For the highest dilution tested, secondary oblique flames running along walls between the main flame front and precursor shock were systematically observed followed by abrupt onset. The widely accepted symmetric assumptions during the very early stages of propagation were confirmed whereas complex asymmetric structures were unraveled and described during FA and DO. The value of simultaneous two-direction high-speed schlieren visualization in providing unique insight into the true reacting front and wave topologies present during the entire DDT evolution was, for the first time, demonstrated. Flame-/shock- boundary layer interactions were a common theme in the cases considered. The maps of spatial likelihood of DO on the channel's cross section showed a strong influence of dilution likely caused by the differences in flow topology prior to transition. The role played by walls and corners in providing the appropriate environment for ignition centers to form was conclusively shown. Future work will employ monoatomic gases as diluents (He or Ar) to investigate compressibility effects on the spatial distribution

of detonation onset.

Acknowledgements

Financial support from the Agence Nationale de la Recherche Program JCJC (FASTD ANR-20-CE05-0011-01) and CPER-FEDER Nouvelle Aquitaine is gratefully acknowledged.

Supplementary material

Videos of simultaneous schlieren visualization for $\eta = 0$ and 2 including early and late stages of flame acceleration, as well as of detonation onset.

References

[1] E. Mallard, H. Le Chatelier, Sur les vitesses de propagation de l'inflammation dans les mélanges gazeux explosifs, Comptes Rendus Hebdomadaires des Séances de l'Académie des Sciences 93 (1881) 145–148.

[2] P. Berthelot, P. Vieille, Nouvelles recherches sur la propagation des phenomenes explosifs dans les gaz, CR Acad. Sci. Paris 95 (1882) 151–157.

[3] P. Wolański, Detonative propulsion, Proceedings of the Combustion Institute 34 (1) (2013) 125–158. doi:doi.org/10.1016/j.proci.2012.10.005.

[4] G. Ciccarelli, S. Dorofeev, Flame acceleration and transition to detonation in ducts, Progress in energy and combustion science 34 (4) (2008) 499–550. doi:doi.org/10.1016/j.pecs.2007.11.002.

[5] I. Moen, J. Lee, The mechanism of transition from deflagration to detonation in vapor cloud explosion, Progress in Energy and Combustion Sciences 6 (1980) 359–389.

[6] Y. B. Zel'Dovich, V. Librovich, G. Makhviladze, G. Sivashinskil, On the onset of detonation in a nonuniformly heated gas, Journal of Applied Mechanics and Technical Physics 11 (2) (1970) 264–270. doi:doi.org/10.1007/BF00908106.

[7] J. E. Shepherd, J. H. Lee, On the transition from deflagration to detonation, in: Major research topics in combustion, Springer, 1992, pp. 439–487. doi:doi.org/10.1007/978-1-4612-2884-4_22.

[8] J. Kurylo, H. Dwyer, A. Oppenheim, Numerical analysis of flowfields generated by accelerating flames, AIAA Journal 18 (3) (1980) 302–308.

[9] B. Deshaies, G. Joulin, Flame-speed sensitivity to temperature changes and the deflagration-to-detonation transition, Combustion and flame 77 (2) (1989) 201–212. doi:doi.org/10.1016/0010-2180(89)90037-0.

[10] K. Shchelkin, Influence of tube roughness on the formation and detonation propagation in gas, Journal of Experimental and Theoretical physics 10 (10) (1940) 823–827.

[11] S. Dorofeev, M. Kuznetsov, V. Alekseev, A. Efimenko, W. Breitung, Evaluation of limits for effective flame acceleration in hydrogen mixtures, Journal of loss prevention in the process industries 14 (6) (2001) 583–589. doi:doi.org/10.1016/S0950-4230(01)00050-X.

[12] M. Ivanov, A. Kiverin, I. Yakovenko, M. A. Liberman, Hydrogen–oxygen flame acceleration and deflagration-to-detonation transition in three-dimensional rectangular channels with no-slip walls, International journal of hydrogen energy 38 (36) (2013) 16427–16440. doi:doi.org/10.1016/j.ijhydene.2013.08.124.

[13] H. Xiao, Q. Duan, J. Sun, Premixed flame propagation in hydrogen explosions, Renewable and Sustainable Energy Reviews 81 (2018) 1988–2001. doi:doi.org/10.1016/j.rser.2017.06.008.

[14] D. Valiev, V. Bychkov, V. Akkerman, L.-E. Eriksson, M. Marklund, Heating of the fuel mixture due to viscous stress ahead of accelerating flames in deflagration-to-detonation transition, Physics Letters A 372 (27-28) (2008) 4850–4857. doi:doi.org/10.1016/j.physleta.2008.04.066.

[15] E. S. Oran, V. N. Gamezo, Origins of the deflagration-to-detonation transition in gas-phase combustion, Combustion and Flame 148 (1-2) (2007) 4–47. doi:doi.org/10.1016/j.combustflame.2006.07.010.

[16] J. Melguizo-Gavilanes, N. Rezaeyan, M. Lopez-Aoyagi, L. Bauwens, Simulation of shock-initiated ignition, Shock Waves 20 (6) (2010) 467–478. doi:doi.org/10.1007/s00193-010-0255-1.

[17] V. N. Gamezo, T. Ogawa, E. S. Oran, Flame acceleration and ddt in channels with obstacles: Effect of obstacle spacing, Combustion and Flame 155 (1-2) (2008) 302–315. doi:doi.org/10.1016/j.combustflame.2008.06.004.

[18] V. N. Gamezo, A. M. Khokhlov, E. S. Oran, The influence of shock bifurcations on shock-flame interactions and ddt, Combustion and flame 126 (4) (2001) 1810–1826. doi:doi.org/10.1016/S0010-2180(01)00291-7.

[19] E. Dziemińska, A. K. Hayashi, Auto-ignition and DDT driven by shock wave–boundary layer interaction in oxyhydrogen mixture, International Journal of Hydrogen Energy 38 (10) (2013) 4185–4193. doi:doi.org/10.1016/j.ijhydene.2013.01.111.

[20] J. Melguizo-Gavilanes, R. Houim, Experimental and numerical study of flame acceleration and transi-

tion to detonation in narrow channels, US National Combustion Meeting, College Park, MD (2017).

[21] M. Liberman, M. Ivanov, A. Kiverin, M. Kuznetsov, A. Chukalovsky, T. Rakhimova, Deflagration-to-detonation transition in highly reactive combustible mixtures, Acta Astronautica 67 (7-8) (2010) 688–701. doi:doi.org/10.1016/j.actaastro.2010.05.024.

[22] V. Bychkov, V. Akkerman, D. Valiev, C. K. Law, Role of compressibility in moderating flame acceleration in tubes, Physical Review E 81 (2) (2010) 026309. doi:doi.org/10.1103/PhysRevE.81.026309.

[23] I. Brailovsky, L. Kagan, G. Sivashinsky, Combustion waves in hydraulically resisted systems, Philosophical Transactions of the Royal Society A: Mathematical, Physical and Engineering Sciences 370 (1960) (2012) 625–646. doi:doi.org/10.1098/rsta.2011.0341.

[24] L. Kagan, G. Sivashinsky, Parametric transition from deflagration to detonation: Runaway of fast flames, Proceedings of the Combustion Institute 36 (2) (2017) 2709–2715. doi:doi.org/10.1016/j.proci.2016.09.026.

[25] J. Melguizo-Gavilanes, Y. Ballossier, L. M. Faria, Experimental and theoretical observations on ddt in smooth narrow channels, Proceedings of the Combustion Institute 38 (3) (2021) 3497–3503. doi:doi.org/10.1016/j.proci.2020.07.142.

[26] Y. Ballossier, F. Virot, J. Melguizo-Gavilanes, Strange wave formation and detonation onset in narrow channels, Journal of Loss Prevention in the Process Industries 72 (2021) 104535. doi:doi.org/10.1016/j.jlp.2021.104535.

[27] Y. Ballossier, F. Virot, J. Melguizo-Gavilanes, Flame propagation and acceleration in narrow channels: sensitivity to facility specific parameters, Shock Waves 31 (4) (2021) 307–321. doi:doi.org/10.1007/s00193-021-01015-9.

[28] D. G. Goodwin, H. K. Moffat, R. L. Speth, Cantera: An object-oriented software toolkit for chemical kinetics, thermodynamics, and transport processes, Caltech, Pasadena, CA (2009).
URL www.cantera.org

[29] S. Browne, J. Ziegler, J. Shepherd, Numerical solution methods for shock and detonation jump conditions, GALCIT report FM2006 6 (2008) 90.

[30] R. Mével, S. Javoy, F. Lafosse, N. Chaumeix, G. Dupré, C. E. Paillard, Hydrogen-nitrous oxide delay time: shock tube experimental study and kinetic modelling, Proceedings of The Combustion Institute 32 (2009) 359–366. doi:doi.org/10.1016/j.proci.2008.06.171.

[31] R. Mével, S. Javoy, G. Dupré, A chemical kinetic study of the oxidation of silane by nitrous oxide, nitric oxide and oxygen, Proceedings of The Combustion Institute 33 (2011) 485–492. doi:doi.org/

10.1016/j.proci.2010.05.076.

[32] S. Bane, J. Ziegler, J. Shepherd, Development of one-step chemistry models for flame and ignition simulation, GALCIT Report GALTCITFM 2010 (2010).

[33] C. Clanet, G. Searby, On the "tulip flame" phenomenon, Combustion and Flame 105 (1-2) (1996) 225–238. doi:doi.org/10.1016/0010-2180(95)00195-6.

[34] V. Bychkov, V. Akkerman, G. Fru, A. Petchenko, L.-E. Eriksson, Flame acceleration in the early stages of burning in tubes, Combustion and Flame 150 (4) (2007) 263–276. doi:doi.org/10.1016/j.combustflame.2007.01.004.

[35] D. M. Valiev, V. Akkerman, M. Kuznetsov, L.-E. Eriksson, C. K. Law, V. Bychkov, Influence of gas compression on flame acceleration in the early stage of burning in tubes, Combustion and Flame 160 (1) (2013) 97–111. doi:doi.org/10.1016/j.combustflame.2012.09.002.

[36] H. Xiao, Q. Duan, L. Jiang, J. Sun, Effects of ignition location on premixed hydrogen/air flame propagation in a closed combustion tube, International Journal of Hydrogen Energy 39 (16) (2014) 8557–8563. doi:doi.org/10.1016/j.ijhydene.2014.03.164.

[37] H. Xiao, R. W. Houim, E. S. Oran, Formation and evolution of distorted tulip flames, Combustion and Flame 162 (11) (2015) 4084–4101. doi:doi.org/10.1016/j.combustflame.2015.08.020.

[38] X. Yang, M. Yu, K. Zheng, P. Luan, S. Han, On the propagation dynamics of lean h2/co/air premixed flame, International Journal of Hydrogen Energy 45 (11) (2020) 7210–7222. doi:doi.org/10.1016/j.ijhydene.2019.12.116.

[39] B. Ponizy, A. Claverie, B. Veyssière, Tulip flame-the mechanism of flame front inversion, Combustion and Flame 161 (12) (2014) 3051–3062. doi:doi.org/10.1016/j.combustflame.2014.06.001.

[40] M. Matalon, C. Cui, J. Bechtold, Hydrodynamic theory of premixed flames: effects of stoichiometry, variable transport coefficients and arbitrary reaction orders, Journal of fluid mechanics 487 (2003) 179–210. doi:doi.org/10.1017/S0022112003004683.

[41] M. Kuznetsov, V. Alekseev, I. Matsukov, S. Dorofeev, Ddt in a smooth tube filled with a hydrogen–oxygen mixture, Shock waves 14 (3) (2005) 205–215. doi:doi.org/10.1007/s00193-005-0265-6.

[42] V. Bykov, A. Koksharov, M. Kuznetsov, V. Zhukov, Hydrogen-oxygen flame acceleration in narrow open ended channels, Combustion and Flame 238 (2022) 111913. doi:doi.org/10.1016/j.combustflame.2021.111913.

[43] I. Brailovskya, G. Sivashinsky, Hydraulic resistance and multiplicity of detonation regimes, Combustion and flame 122 (1-2) (2000) 130–138. doi:doi.org/10.1016/S0010-2180(00)00108-5.

[44] M. Kuznetsov, M. Liberman, I. Matsukov, Experimental study of the preheat zone formation and deflagration to detonation transition, Combustion Science and Technology 182 (11-12) (2010) 1628–1644. doi:doi.org/10.1080/00102202.2010.497327.

[45] P. Krivosheyev, O. Penyazkov, A. Sakalou, Analysis of the final stage of flame acceleration and the onset of detonation in a cylindrical tube using high-speed stereoscopic imaging, Combustion and Flame 216 (2020) 146–160. doi:doi.org/10.1016/j.combustflame.2020.02.027.

[46] A. Y. Poludnenko, T. A. Gardiner, E. S. Oran, Spontaneous transition of turbulent flames to detonations in unconfined media, Physical Review Letters 107 (5) (2011) 054501. doi:doi.org/10.1103/PhysRevLett.107.054501.

[47] T. Machida, M. Asahara, A. K. Hayashi, N. Tsuboi, Three-dimensional simulation of deflagration-to-detonation transition with a detailed chemical reaction model, Combustion Science and Technology 186 (10-11) (2014) 1758–1773. doi:doi.org/10.1080/00102202.2014.935647.

[48] P. Urtiew, A. Oppenheim, Experimental observations of the transition to detonation in an explosive gas, Proceedings of the Royal Society of London. Series A. Mathematical and Physical Sciences 295 (1440) (1966) 13–28. doi:doi.org/10.1098/rspa.1966.0223.

[49] P. Clavin, H. Tofaili, A one-dimensional model for deflagration to detonation transition on the tip of elongated flames in tubes., Combustion and Flame 232 (2021) 111522. doi:doi.org/10.1016/j.combustflame.2021.111522.

[50] J. Melguizo-Gavilanes, L. Bauwens, An experimentally informed 1-D DDT model for smooth narrow channels, in: 28th Int. Colloquium on the Dynamics of Explosions and Reactive Systems (ICDERS), Napoli, ITA, 2022.

[51] Y. B. Zeldovich, Regime classification of an exothermic reaction with nonuniform initial conditions, Combustion and Flame 39 (2) (1980) 211–214. doi:doi.org/10.1016/0010-2180(80)90017-6.

[52] A. D. Kiverin, D. R. Kassoy, M. F. Ivanov, M. A. Liberman, Mechanisms of ignition by transient energy deposition: Regimes of combustion wave propagation, Physical Review E 87 (3) (2013) 033015. doi:doi.org/10.1103/PhysRevE.87.033015.

[53] D. Valiev, V. Bychkov, V. Akkerman, L.-E. Eriksson, C. K. Law, Quasi-steady stages in the process of premixed flame acceleration in narrow channels, Physics of Fluids 25 (9) (2013) 096101. doi:doi.org/10.1063/1.4819885.